ZhangFei Su, Muzaffar Shodiev, J. Jay Leitch, Fatemeh Abbasi, and Jacek Lipkowski, The role of transmembrane potential and defects on permeabilization of lipid bilayers by alamethicin, an ion channels forming peptide, *Langmuir*, **2018**,*34*,6249-6260

# The role of transmembrane potential and defects on the permeabilization of lipid bilayers by alamethicin, an ion channel forming peptide

ZhangFei Su[&], Muzaffar Shodiev[&], J. Jay Leitch, Fatemeh Abbasi, and Jacek Lipkowski[*]

*Department of Chemistry, University of Guelph, Guelph, Ontario N1G 2W1, Canada*

& Two authors contribute equally to the paper

* E-mail: jlipkows@uoguelph.ca

## Abstract

The insertion and ion conducting channel properties of alamethicin reconstituted into a 1, 2-di-O-phytanyl-*sn*-glycero-3-phosphatidylcholine (DPhPC) bilayer floating on the surface of gold (111) electrode modified with a 1-thio-$\beta$-D-glucose ($\beta$-Tg) self-assembled monolayer were investigated using a combination of electrochemical impedance spectroscopy (EIS) and polarization modulation infrared reflection absorption spectroscopy (PM-IRRAS). The hydrophilic $\beta$-Tg monolayer separated the bilayer from the gold substrate and created a water-rich spacer region, which better represents natural cell membranes. The EIS measurements acquired information about the membrane resistivity (a measure of membrane porosity) and the PM-IRRAS experiments provided insight into the conformation and orientation of the membrane constituents as a function of the transmembrane potential. The results showed that the presence of alamethicin had a small effect on the conformation and orientation of phospholipid molecules within the bilayer for all studied potentials. In contrast, the alamethicin peptides assumed a surface state, where the helical axes adopted a large

tilt angle with respect to the surface normal, at small transmembrane potentials and inserted into the bilayer at sufficiently negative transmembrane potentials forming pores, which behaved as barrel-stave ion channels for ionic transport across the membrane. The results indicated that insertion of alamethincin peptides into the bilayer was driven by the dipole-field interactions and that the transition to and from the inserted to surface states were electrochemically reversible. Additionally, the EIS measurements performed on phospholipid bilayers without alamethicin showed that the application of negative transmembrane potentials also introduces defects into the bilayer. The membrane resistances measured in both the absence and presence of alamethicin show similar dependences on the electrode potential suggesting that the insertion of the peptide may also be assisted by the electroporation of the membrane. The findings in this study provide new insights into the mechanism of alamethicin insertion into phospholipid bilayers.

**Keywords:** alamethicin, ion channels, floating bilayer, EIS, PM-IRRAS

## 1. Introduction

Antimicrobial peptides (AMPs) are an integral part of the innate immune system, which is responsible for defending an organism against invading pathogenic bacteria. AMPs preferentially bind to bacterial cells making them highly toxic towards a broad range of Gram positive and Gram negative bacteria, while remaining harmless towards mammalian cells. The mechanism of AMP activity involves the attachment and insertion of the peptides into bacterial cytoplasmic membranes to form transmembrane pores.[1] For the above reasons, AMPs make excellent candidates for the future generation of antimicrobial drugs to combat the growing number of antibiotic resistant bacterial strains.[2] Consequently, the relationships between the structure and activity of both natural and synthetic AMPs are widely studied to develop novel AMP antibiotics with improved properties.[3]

Alamethicin (Alm) is a linear antimicrobial peptide consisting of 20 amino acid

residues produced by the fungus *Trichoderma viride*.[4] Alamethicin behaves as a voltage-gated ion channel in lipid bilayers and biological cell membranes.[5] It is composed of a high proportion of the non-proteinogenic amino acid residue Aib (2-aminoisobutyric acid), which strongly induces the formation of a helical structure. X-ray diffraction (XRD) studies of alamethicin determined that the structure of alamethicin is predominantly helical with a $\alpha$-helix at the N-terminus and a $3_{10}$-helix at the C-terminus. The transition from the $\alpha$-helix to the $3_{10}$-helix occurs at the Pro14 residue,[6] which creates a slight bend in the overall helical structure. Due to the readily available crystallographic data, alamethicin has served as an ideal model for studying the mechanism of voltage-gated ion channels.[7]

The structure, conformation and orientation of alamethicin in biomimetic lipid membranes have been widely researched. Huang's group found that alamethicin forms barrel-stave ion channels in a variety of different lipid bilayers using neutron scattering and circular dichroism (CD) methods.[8, 9] The orientation of alamethicin in the membrane depends on its concentration. At low peptide-to-lipid ratios (P/L), the helical axis of alamethicin is aligned parallel to the surface plane of the bilayer (surface state). When the P/L concentration becomes sufficiently large and exceeds the critical value (P/L*) of the phospholipid membrane, alamethicin peptides insert into the lipid bilayer with the helical axis assuming a small angle with respect to the normal of the bilayer plane (inserted state).[10] The effect of lipid chain length and their phase behavior (gel or liquid crystalline) on alamethicin insertion has been investigated by Pan et al.[11] and Salditt et al.[12, 13, 14], who found that the aggregation of alamethicin is strongly dependent on the thickness and physical state of the bilayer. Becucci and Guidelli employed electrochemical impedance spectroscopy (EIS) to study the ion channel properties of alamethicin in a tethered lipid bilayer on mercury electrode surfaces. They proposed that the insertion of the alamethicin peptides into the bilayer was driven by dipole-field interactions, which results in the formation of ion conducting pores via aggregation of the inserted Alm monomers.[15, 16] Marsh used the spin-label electron paramagnetic resonance (EPR) to determine the orientation of alamethicin in different lipid bilayers and discovered that the tilt angle of the helix

decreased as the lipid chain length was increased.[17] Bak et al.[18] applied solid-state NMR to study different $^{15}$N-labeled alamethicin in DMPC membranes and demonstrated that alamethicin mainly behaved as a linear helical structure spanning the lipid membrane with the helix axis tilted by 10$^{o}$ to 20$^{o}$ relative to the bilayer surface normal. Chen's research group studied the orientation of alamethicin in a series of lipid bilayers using sum frequency generation (SFG) and attenuated total internal reflection (ATR) spectroscopies.[19, 20, 21, 22] They reported that the alamethicin molecules were located on surface of the POPC bilayer (surface state) in neutral pH solutions, and inserted into the bilayer when alkaline solutions were introduced.[20] Additionally, these researchers also found that the peptides were inserted into the lipid bilayer when it exists in a liquid crystalline state and returned to the surface state when the phospholipids transitioned to the gel state.[21, 22] Scanning tunneling microscopy (STM) images obtained by Pieta et al.[23] provided the first direct visualization of the alamethicin aggregates in a phospholipid monolayer supported at a gold electrode surface. More recently, Abbasi et al.[24] employed atomic force microscopy (AFM) to attain images of the alamethicin pores in a floating bilayer lipid membrane (fBLM).

It has been well-established that alamethicin forms voltage-gated ion channels, but the voltage-gated behavior has primarily been investigated by electrochemical techniques.[15, 16] Therefore, it is important to verify the voltage-gated models using spectroscopic techniques, which provide direct information about the changes in the orientation and conformation of the peptide as a function of the transmembrane potential. Recently, Forbrig et al.[25] employed surface enhanced infrared reflection absorption spectroscopy (SEIRAS) to monitor the incorporation of alamethicin into a model membrane supported on a gold coated ATR element. SEIRAS studies of model biological membranes were also performed by Ataka et al.[26] Independently, we have investigated model membranes supported on gold (111) electrode surfaces.[27, 28] In these systems, the transmembrane potential was recorded and the electric field driven structural changes in the membrane were studied using infrared reflection absorption spectroscopy (IRRAS). Recently, we have described ion channels properties of

alamethicin in 1,2-di-O-phytanyl-*sn*-glycero-3-phosphocholine (DPhPC) bilayers directly deposited on the gold (111) electrode surface (sBLM).[29] In this architecture, the gold substrate applies stress to the bilayer and this stress may affect the properties of alamethicin molecules. To eliminate the surface stress on the bilayer, we have performed measurements on a tethered bilayer lipid membrane (tBLM) where the membrane was separated from the metal surface by a hydrophilic spacer.[30] This model was successful at alleviating the surface stress, however, the mobility of alamethicin molecules in the tethered bilayer was significantly reduced and peptide insertion showed no voltage-gated behavior. In the present paper, the third in this series, we have employed a floating bilayer (fBLM) to understand the differences between the behaviors of alamethicin in different types of biomimetic membranes. The gold electrode surface was modified with a self-assembled monolayer (SAM) of 1-thio-$\beta$-D-glucose ($\beta$-Tg). A DPhPC bilayer containing alamethicin at a concentration of 10 mol% was then deposited on top of the $\beta$-Tg monolayer using the Langmuir-Blodgett/Langmuir-Schaefer techniques. The architecture of the floating bilayer is shown in Figure 1 (A) and schematic structures of its constituents are presented in Figure 1 (B). The $\beta$-Tg SAM offered a hydrophilic environment that protects the structure and organization of the peptides and lipids in the floating bilayer from the solid substrate.[31, 32] Electrochemical and PM-IRRAS techniques were used to study properties of alamethicin in the floating bilayer as a function of the electrode potential. The difference between the applied potential and potential of zero free charge of the electrode covered by the fBLM ($E$-$E_{\mathrm{pzfc}}$) was used as a measure of the transmembrane potential. The results of this work reveal the relationship between the transmembrane potential of the lipid bilayer and the presence of alamethicin in either the surface or inserted states. This study provides unique information about the voltage-driven insertion of this peptide into the bilayer. By comparing the behavior of alamethicin in sBLM, tBLM and fBLM systems, we were able to demonstrate that insertion of the peptide was facilitated by defects in the bilayer and that these defects can be created by the applied transmembrane potential. This finding has more general implications since it provides important information how to facilitate the

reconstitution of peptides into model membranes.

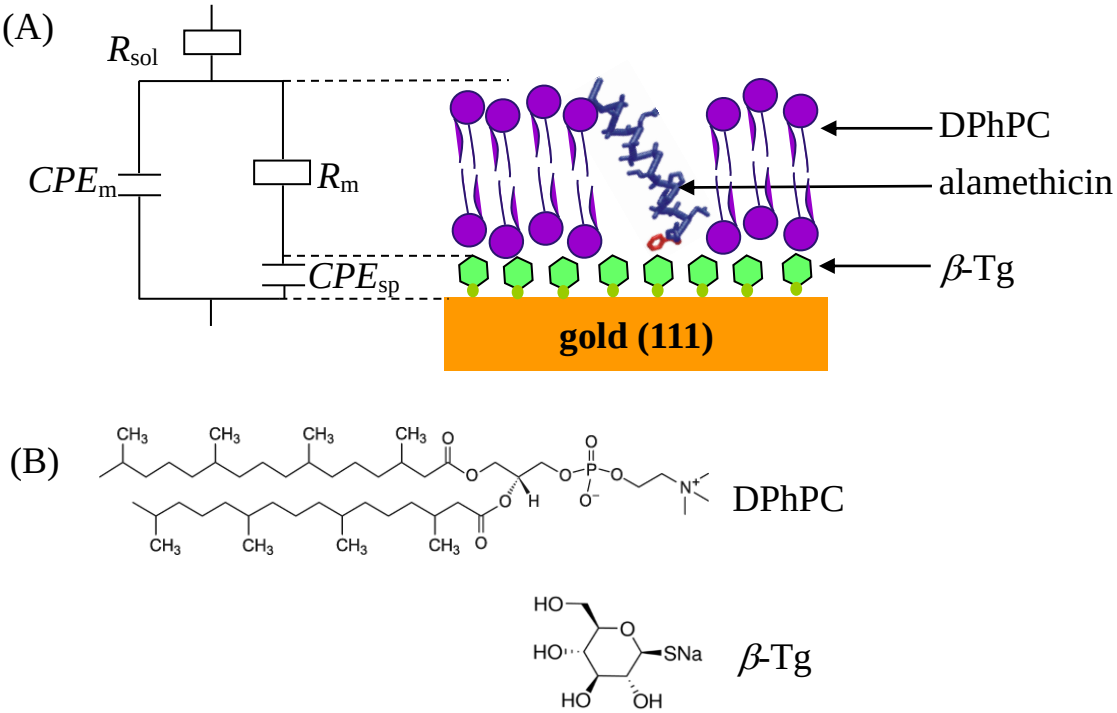


Figure 1. (A) Schematic diagram of the DPhPC/Alm floating bilayer on the *β*-Tg modified gold (111) surface. The equivalent circuit used to model the EIS data is shown on the left. (B) Chemical structure of DPhPC and *β*-Tg.

## 2. Experiment

### 2.1 Materials

Alamethicin (Alm) from *Trichoderma viride* (98%), 1-thio-*β*-D-glucose sodium salt (*β*-Tg), deuterium oxide (99.9 atom % D) and sodium fluoride (Bioxtra, >99%) were purchased from Sigma-Aldrich. 1,2-di-*O*-phytanyl-*sn*-glycero-3-phosphocholine (DPhPC) was obtained from Avanti Polar Lipids. The NaF powder was cleaned in an ultraviolent ozone chamber (UVO cleaner, Jelight, Irvine, CA) for 20 minutes to oxidize any organic impurities before use. All other chemicals were used without further purification. All aqueous solutions were prepared from the ultrapure water purified by a Milli-Q (Millipore, Bedford, MA) water system (resistivity > 18.2 MΩ cm).

The single crystal gold (111) electrodes, which were grown, oriented and cut in

our laboratory,[33] were used as the working electrodes in the electrochemical and PM-IRRAS experiments. Prior to every experiment, the gold (111) electrode was flame annealed and cooled in air under the plume of the flame. All potentials reported in this paper are quoted versus the Ag/AgCl (saturated KCl) electrode. All experiments were performed at room temperature (20 ± 2 $^{o}$C).

### 2.2 Assembly of the DPhPC/Alm (9:1) floating bilayers on $\beta$-Tg modified gold (111) surface

The gold (111) electrode was flame annealed and then immersed in a 2 mM $\beta$-Tg sodium salt solution in methanol (Fisher Scientific, HPLC grade) over night. Afterwards, the electrode was thoroughly rinsed with methanol to remove physically adsorbed $\beta$-Tg molecules followed by ultrapure water to remove residual methanol.

The combination of Langmuir-Blodgett (LB) and Langmuir-Schaefer (LS) techniques was used to deposit the DPhPC/Alm (9:1, mol ratio) bilayer on top of the $\beta$-Tg SAM at the gold (111) surface. The bilayer was transferred at a surface pressure of 30 mN m$^{-1}$. Additional details about the deposition of the bilayer were given in Ref. [29].

### 2.3 Electrochemical instrument and measurements

The immersion method was employed to determine the potential of zero free charge ($E_{pzfc}$) of the DPhPC/Alm floating bilayers on the $\beta$-Tg modified gold (111) surface.[34, 35] The procedure of these measurement were described in Ref. [35].

The EIS measurements were performed using the Solartron SI 187 electrochemical interface and Solartron SI 1260 impedance/gain-phase analyzer. Spectra were collected for frequencies ranging from $10^{-2}$ to $10^{3}$ Hz with the excitation amplitude of 10 mV. The data analysis of the EIS results was performed in the ZView software (Scribner Associates Inc.).

### 2.4 PM-IRRAS measurement

PM-IRRAS experiments were performed using a Thermo Nicolet Nexus 870

spectrometer (Madison, WI), equipped with an external tabletop optical mount (TOM) box. A 1 inch $CaF_2$ equilateral prism (BoXin, Changchun, CN) was used as the IR window. The PM-IRRAS spectra were measured with the photoelastic modulator (PEM) set for half-wave retardation at 1600 $cm^{-1}$ for the amide I band region and 2900 $cm^{-1}$ for the C-H stretching region. The angle of incidence was set to 60° for amide I band region and 57° for the C-H stretching region to obtain a large enhancement of the mean square electric field strength (MSEFS) of the *p*-polarized radiation on the electrode surface. $D_2O$ solution was employed to avoid IR absorption by $H_2O$ around 1650 $cm^{-1}$ and 2900 $cm^{-1}$ regions. At each potential, 4000 IR scans were added and averaged with the instrumental resolution of 4 $cm^{-1}$. The detailed information about the PM-IRRAS measurements was given in Ref. [28].

### 2.5 Calculation of the tilt angle

The PM-IRRAS spectra of the DPhPC/Alm floating bilayer with randomly oriented molecules can be simulated using a model of five homogeneous, parallel phases (Au/$\beta$-Tg/(DPhPC/Alm)/$D_2O$/$CaF_2$) and custom written software that solves Fresnel equations with the help of the transfer matrix method.[36] The average tilt angles of the $3_{10}$-helix ($\gamma(3_{10}$-helix)) and $\alpha$-helix ($\gamma(\alpha$-helix)) in alamethicin, as well as the average tilt angles of the trans fragments of the diphytanyl chains ($\gamma_{chain}$) and the average angle of the transition dipole moment of the C=O bond ($\theta_{CO}$) with respect to the surface normal for the DPhPC molecules are calculated from the integrated intensity of the corresponding IR bands of the experimentally measured and simulated PM-IRRAS spectra. Details concerning the spectra simulation and tilt angles calculation were described in Ref. [29].

## 3. Results and Discussion

### 3.1 Electrochemical data

When a film of organic molecules contains chemisorbed thiols ($\beta$-Tg in this case), one has to distinguish between the potential of zero total charge ($E_{pztc}$) and the

potential of zero free charge ($E_{pzfc}$). The physical meaning of $E_{pztc}$ and $E_{pzfc}$ was discussed in Ref [35]. The $E_{pztc}$ corresponds to the potential where the surface energy reaches a maximum (i.e. maximum on the electrocapillary curve). The $E_{pzfc}$ corresponds to zero free charge on the metal surface and zero charge in the diffuse part of the double layer. In the presence of chemisorb thiols, $E_{pztc}$ and $E_{pzfc}$ are not equal. The immersion method was applied to determine the potential of zero free charge of the pure DPhPC and DPhPC/Alm floating lipid bilayers by plotting the free charge at the electrode surface ($\sigma_M$) as a function of the immersion potential as shown in Figure 2. Figure S1 in the Supporting Information shows two representative current transients measured when the $\beta$-Tg modified gold (111) electrode covered by the DPhPC/Alm bilayer was brought in contact with the 0.1M NaF solution at a controlled immersion potential. These current transients were integrated to calculate the charges plotted in Figure 2. A freshly prepared fBLM was used for each immersion potential. The error bars correspond to the upper and lower values of two independent measurements. Negative transients were recorded when the immersion potential was lower than the $E_{pzfc}$ and positive transients when the immersion potential was higher than $E_{pzfc}$. The linear regression of the free charge density data gives the potential of zero free charge where $E_{pzfc}$ = 0.18 ± 0.03 V vs. Ag/AgCl for the DPhPC/Alm floating bilayer and $E_{pzfc}$ = 0.22 ± 0.02 V vs. Ag/AgCl for the pure DPhPC floating bilayer (without alamethicin). The $E_{pzfc}$ of the DPhPC/Alm bilayer is ~0.04 V lower than $E_{pzfc}$ of the DPhPC bilayer. For bilayers directly supported at the gold (111) electrode (without SAM of $\beta$-Tg ), the $E_{pzc}$ was equal to 0.10 ± 0.02 V vs. Ag/AgCl for the DPhPC/Alm bilayer and 0.20 ± 0.02 V vs. Ag/AgCl for the pure DPhPC bilayer.[29] The $E_{pzfc}$ of the $\beta$-Tg monolayer at the gold (111) surface was determined to be 0.28 ± 0.03 V vs. Ag/AgCl,[35] and the $E_{pzc}$ for film-free, pure gold (111) surface is equal to 0.30 ± 0.02 V vs. Ag/AgCl. The values of $E_{pzfc}$ for the DPhPC/Alm and DPhPC bilayers are more negative than that for the pure gold electrode. This is consistent with the general trend of a negative shift in the $E_{pfzc}$ of the gold (111) electrode in the presence of the phospholipid bilayers.[37]

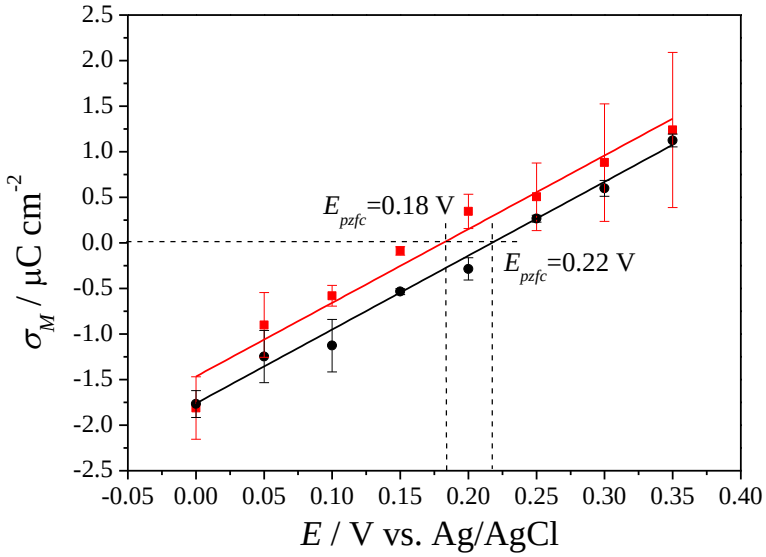


Figure 2. The double layer charge of the pure DPhPC floating bilayer (black) and DPhPC/Alm floating bilayer (red) on the *β*-Tg modified gold (111) electrode in 0.1 M NaF electrolyte are plotted as a function of the immersion potential. The dashed lines denote the positions of the $E_{pzc}$ for the two systems.

Next, EIS measurements were performed to determine the conductivity/resistivity of the DPhPC/Alm fBLM. Figure 3 plots the absolute values of the impedance and phase angles of the DPhPC/Alm fBLM coated gold (111) electrode as a function of the frequency measured at different potentials. The EIS spectra were fitted to the equivalent circuit depicted in Figure 1 (A), which was previously proposed by Valincius et al.[38, 39, 40, 41, 42]). In this model, $R_{sol}$ is the resistance of the electrolyte; $R_m$ and $CPE_m$ are the resistance and constant phase element of the lipid bilayer, respectively. $CPE_{sp}$ is the constant phase element of the spacer region, which describes the electrochemical behavior of the *β*-Tg SAM and water layer separating the bilayer from the gold electrode surface. Constant phase elements were employed in the equivalent circuit to account for the heterogeneity of the floating bilayer and the spacer region. The impedance of the CPE can be expressed as:

$$Z_{CPE} = \frac{1}{Q(j\omega)^{\alpha}} \quad (1)$$

where $Q$ is the constant phase element coefficient measured in μF $cm^{-2}$ $s^{\alpha-1}$ and α is related to the frequency dispersion. EIS data were collected by negatively stepping the potential from the $E_{pzfc}$ to -0.6 V vs. Ag/AgCl where lifting of the bilayer from the gold surface begins to occur.

The numerical values of the equivalent circuit elements for the DPhPC/Alm bilayers at different potentials determined from the EIS measurement are listed in Table 1. Since the empirical constant $\alpha_m$ is close to 1, $Q_m$ can be treated as the capacitance of the DPhPC/Alm bilayer. For majority of potentials, the numerical values of $\alpha_{sp}$ are close to 0.5. According to Valincius et al.[41, 42], this indicates that the number of defects/pores is considerably low and that the defects/pores are sufficiently isolated meaning that the flux of ions penetrating through individual pores do not overlap in the submembrane (spacer) region. For the EIS data recorded at potentials of -0.1V and -0.6V vs. Ag/AgCl, the values of $\alpha_m$ are 0.73 ± 0.04 and 0.36 ± 0.04, respectively. These numbers have no clear physical meaning and indicate the data of the spacer region may be affected by larger errors. However the $R_m$ are consistent with values reported for other potentials.

Complementary EIS results for the pure DPhPC floating bilayer at selected electrode potentials are shown in Figure S2 of the Supporting Information. The numerical values of the equivalent circuit elements for the DPhPC bilayers without alamethicin at different potentials are listed in Table S1 and Table S2. The discussion of the model chosen for the data analysis of the DPhPC bilayers is given in Figure S3.

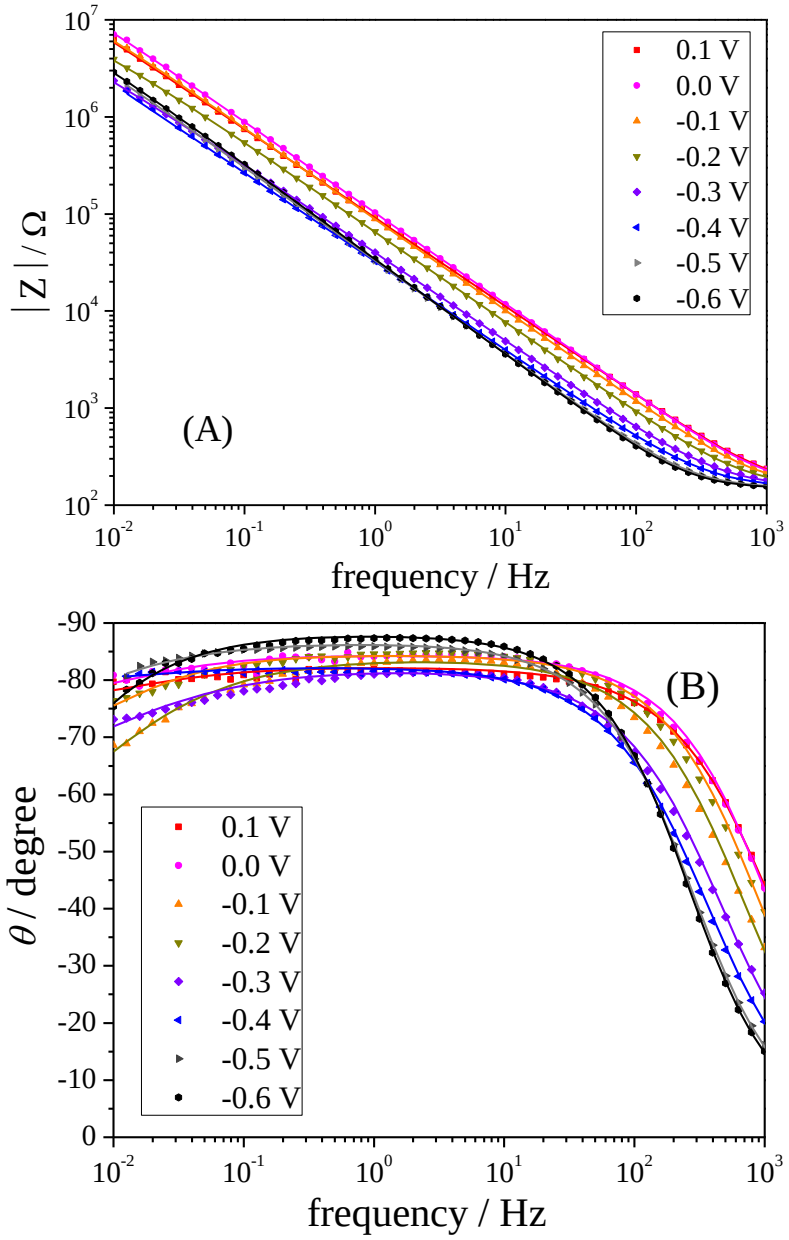


Figure 3. EIS results of the DPhPC/Alm bilayer floating on the $\beta$-Tg modified gold (111) surface in a 0.1 M NaF at different potentials vs Ag/AgCl showing the (A) absolute magnitude of the impedance and (B) phase angle as a function of the frequency. The symbols represent the measured data and the solid lines represent the fits obtained by the equivalent circuit, presented in Figure 1 (A), using the numerical values of the equivalent circuit listed in Table 1.

Figure 4 (A) plots the $Q_m$ values of the DPhPC floating bilayer in the absence (black) and presence (red) of alamethicin. The top horizontal axis of Figure 4 presents

the difference between the applied potential ($E$) and the potential of zero free charge ($E_{pzfc}$) for DPhPC/Alm bilayer. This potential difference is an approximate measure of the transmembrane potential. The two floating bilayers are stable in the potential region between 0.1 V and -0.6 V vs. Ag/AgCl electrode. The instability of these films outside of this potential window is caused by the onset of $OH^-$ adsorption (pH = 8.4 in 0.1 M NaF solution), which occurs at potentials more positive than 0.1 V vs. Ag/AgCl, and by desorption of the DPhPC and DPhPC/Alm films at potentials more negative than -0.6 V vs. Ag/AgCl.

Table 1. Numerical values of the elements in the equivalent circuit of the DPhPC/Alm floating bilayer on the $\beta$-Tg modified gold (111) surface in 0.1 M NaF at different electrode potentials.

| $E$ / V vs. Ag/AgCl | $Q_m$ / μF $cm^{-2}$ $s^{\alpha-1}$ | $\alpha_m$ | $R_m$ / MΩ $cm^2$ | $Q_{sp}$ / μF $cm^{-2}$ $s^{\alpha-1}$ | $\alpha_{sp}$ |
|---|---|---|---|---|---|
| 0.1 | 9.8 ± 0.7 | 0.920 ± 0.008 | 8.6 ± 1.1 | 0.79 ± 0.05 | 0.63 ± 0.04 |
| 0.0 | 7.9 ± 0.3 | 0.944 ± 0.009 | 9.1± 0.9 | 0.93 ± 0.11 | 0.64 ± 0.1 |
| -0.1 | 8.9 ± 0.4 | 0.942 ± 0.004 | 5.4 ± 0.6 | 2.6 ± 0.26 | 0.73 ± 0.04 |
| -0.2 | 11.5 ± 1.5 | 0.933 ± 0.004 | 1.0 ± 0.3 | 2.3 ± 0.53 | 0.49 ± 0.1 |
| -0.3 | 17.4 ± 2.7 | 0.922 ± 0.017 | 0.79 ± 0.3 | 2.4 ± 0.24 | 0.52 ± 0.08 |
| -0.4 | 22.4 ± 2.5 | 0.931 ± 0.021 | 1.8 ± 0.2 | 1.5 ± 0.20 | 0.61 ± 0.08 |
| -0.5 | 21.7 ± 2.4 | 0.965 ± 0.004 | 1.7 ± 0.2 | 1.1 ± 0.13 | 0.53 ± 0.16 |
| -0.6 | 20.7 ± 1.8 | 0.984 ± 0.006 | 1.5 ± 0.2 | 1.7 ± 0.16 | 0.36 ± 0.07 |

The $Q_m$ curves display a minimum at ($E$-$E_{pzfc}$) ~ -0.2 V, which equates to minimum capacitance values of ~8.0 μF $cm^{-2}$ $s^{\alpha-1}$ for both floating bilayer systems. The low values of $Q_m$ for the DPhPC/Alm bilayers are maintained when the transmembrane potential is between 0 and -0.3 V, and apparently increases when the transmembrane potential is more negative than -0.3 V. The overall shape of the $Q_m$

curve for the pure DPhPC bilayer is similar to the DPhPC/Alm bilayer although the low capacitance region is shifted by ~0.1 V in negative direction.

In the transmembrane potentials range between -0.4 V and -0.8 V, $Q_m$ increases and attains values between ~12 and ~22 μF cm$^{-2}$ s$^{\alpha-1}$. Below, we will demonstrate that this increase in capacitance is due to the insertion of alamethicin into the biomimetic membrane. The bilayer undergoes electroporation in this potential range allowing water to incorporate into the membrane.[43, 44] The bilayers are then lifted from the surface when voltages more negative than -0.8 V are applied to the modified gold (111) electrode.

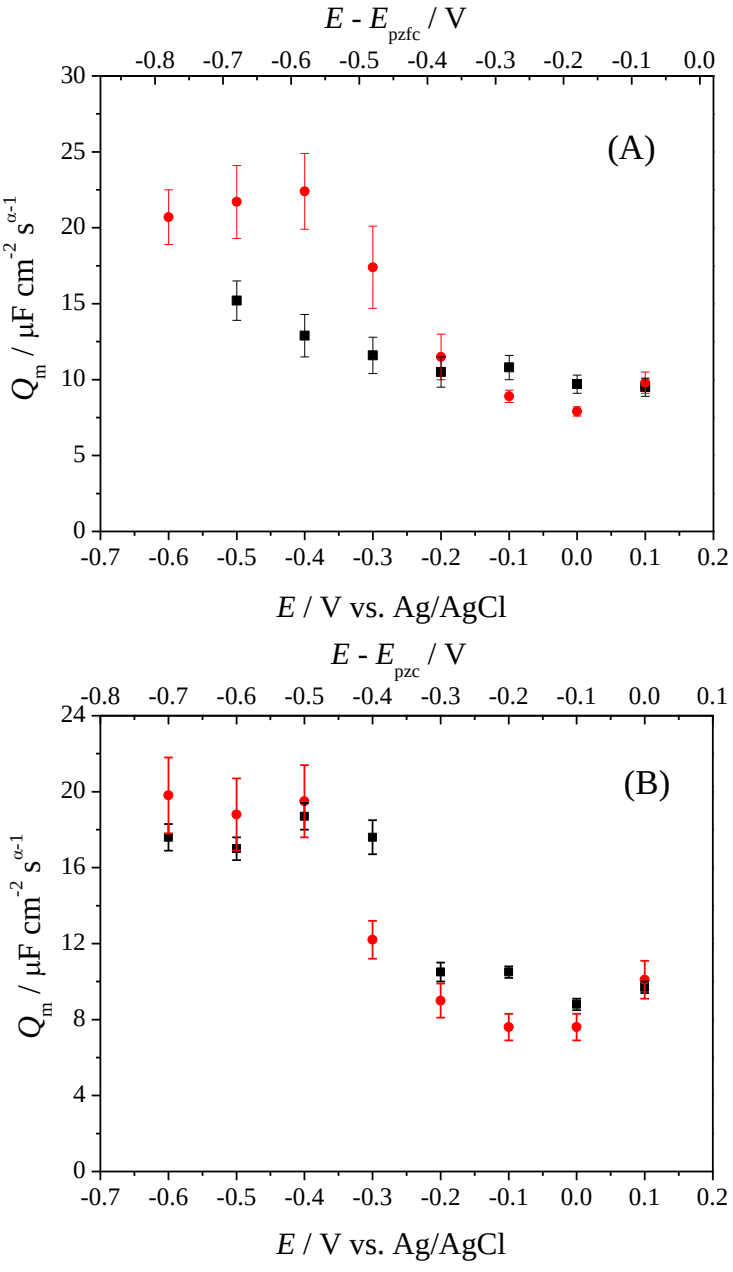

Figure 4. Constant phase element coefficient ($Q_m$) of DPhPC (black rectangles) and DPhPC/Alm (red circles) (A) fBLMs at $\beta$-Tg modified gold (111) surface and (B) sBLM at the gold (111) surface.

In a recent paper, we have investigated the potential controlled insertion of alamethicin into the DPhPC/Alm bilayer directly supported at the gold (111) electrode surface (in the absence of the hydrophilic SAM of $\beta$-Tg).[29] At that time, the impedance measurements were only performed on the DPhPC/Alm bilayer. In view of the potential dependent changes in membrane resistivity observed in this work with the pure DPhPC fBLM, we revisited that study and performed EIS measurements on DPhPC bilayer directly supported on the gold (111) surface (sBLM) in the absence of alamethicin. The numerical values of the equivalent circuit elements obtained from the fit to the data are given in Tables S3 and S4 for sBLMs in the presence and absence of alamethicin, respectively.

Figure 4 (B) plots the $Q_m$ values determined for DPhPC and DPhPC/Alm bilayers deposited directly onto the gold electrode surface. The $Q_m$ curves of the sBLMs in Figure 4 (B) have similar shapes to the curves of the fBLMs in Figure 4 (A). The major difference between these two model membranes is that the onset of $OH^-$ adsorption occurred earlier (i.e. less positive potentials) in the sBLMs. Apparently, the presence of the SAM of $\beta$-Tg in fBLMs inhibits the penetration of the $OH^-$ ion at positive potentials. The minimum values of $Q_m$ were ~8.0 μF $cm^{-2}$ $s^{\alpha-1}$ for the both sBLMs (absence and presence of Alm), which are also similar to the minimum values of $Q_m$ attained for the two fBLMs presented in Figure 4 (A), suggesting that polar heads of DPhPC in the leaflet in contact with the metal are quite hydrated in the sBLM.

Figure 5 (A) compares the $R_m$ values for the fBLMs with and without alamethicin as a function of the applied potential. The values of $R_m$ for both bilayers decrease when the applied potential becomes negative (or when ($E$ - $E_{pzfc}$) < -0.2 V). This decrease in $R_m$ correlates with the increase in $Q_m$ observed in Figure 4 and correspond to the onset of bilayer electroporation previously observed by neutron

reflectivity[43] and SEIRAS[44] measurements. It should be noted that the $R_m$ values of the DPhPC/Alm bilayer are always lower than $R_m$ of the DPhPC bilayer implying that the incorporation of Alm leads to overall an increase in the number and/or size of the defects found within the membrane.

The membrane resistances of the DPhPC and DPhPC/Alm sBLMs, obtained from the EIS measurements, are plotted as a function of the applied voltage in Figure 5 (B). The trends observed for the sBLM systems are very similar to the trends recorded in the fBLM films presented in Figure 5 (A). Figures 5 (A) and (B) show that the changes in the $R_m$ values in the presence of alamethicin are correlated to the changes in the $R_m$ values in the absence of alamethicin. To determine whether this behavior is due to an increase in the number of defects or the formation of ion conducting pores, PM-IRRAS measurements were performed. In the following investigation, we will first examine the behavior of the phospholipid acyl chains before discussing the properties of alamethicin molecules to decouple the effects of these two individual membrane components.

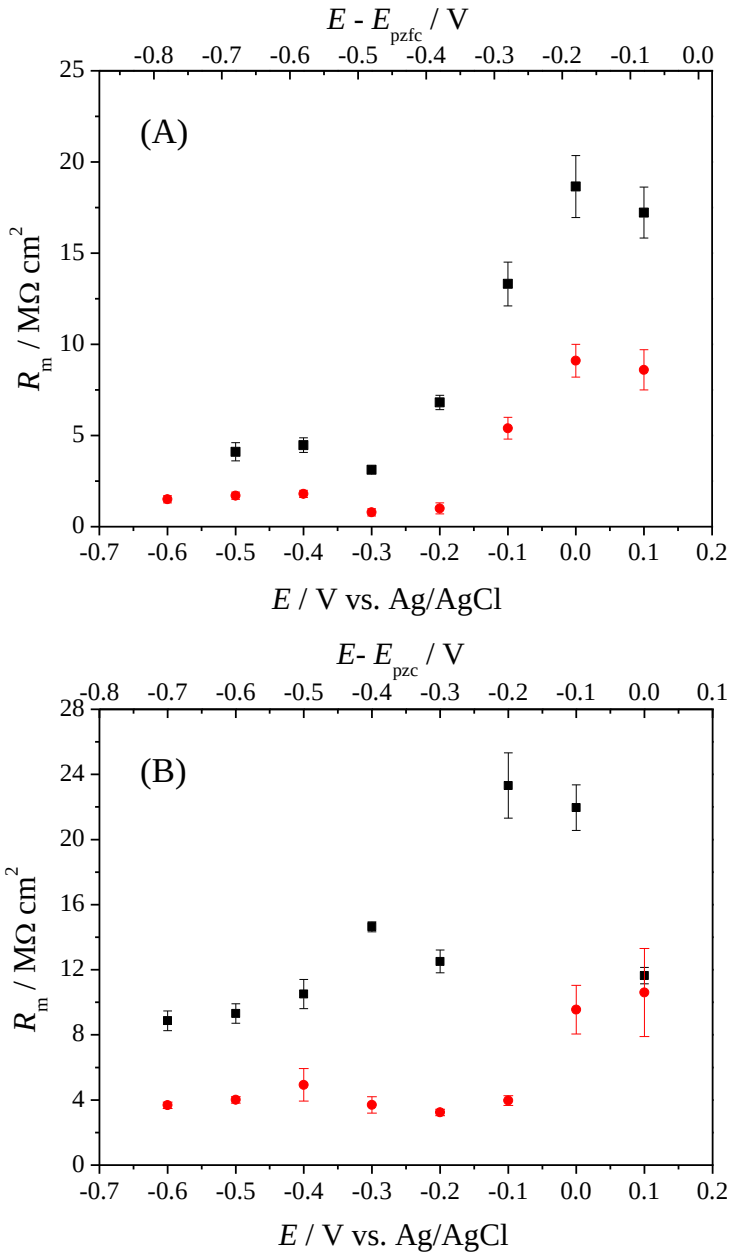


Figure 5. Variation of the membrane resistance ($R_m$) of the DPhPC (black rectangles) and DPhPC/Alm (red circle) in the (A) fBLMs and (B) sBLMs as a function the applied potential (lower potential axis). The upper potential scale represents a difference between applied $E$ and $E_{pzfc}$ of the DPhPC/Alm bilayers.

### 3.2 PM-IRRAS measurements

#### 3.2.1 Acyl chain region

PM-IRRAS spectra of the DPhPC/Alm floating bilayers in the C-H stretching

region are plotted in Figure 6. These bands primarily originate from vibrations of the DPhPC diphytanyl chains and provide information about the orientation and conformation of the lipid tails. The intensity of the C-H stretching bands is nearly potential independent. The IR band deconvolution was performed using the procedure used described in Ref. [45] and the band assignment was supported by DFT calculations.[45] The peak center of the $CH_2$ symmetric stretching ($\nu_s(CH_2)$) and $CH_2$ asymmetric stretching ($\nu_{as}(CH_2)$) in the DPhPC/Alm bilayer are located at 2859 ± 2 $cm^{-1}$ and 2930 ± 2 $cm^{-1}$, respectively. In the gel state, the IR peak positions of $\nu_s(CH_2)$ and $\nu_{as}(CH_2)$ should be below 2850 and 2920 $cm^{-1}$, respectively, since the acyl chains of lipid molecules are fully stretched and assume an all *trans* conformation.[46] Shifts to higher frequencies indicate that the methylene bands of the lipid tails within the bilayer are in a liquid crystalline state. For DPhPC, the transition temperature of the gel to liquid crystalline state for DPhPC occurs at -120℃.[47] Hence, the high frequencies of the methylene bands are consistent with the fluid state of the DPhPC bilayer.

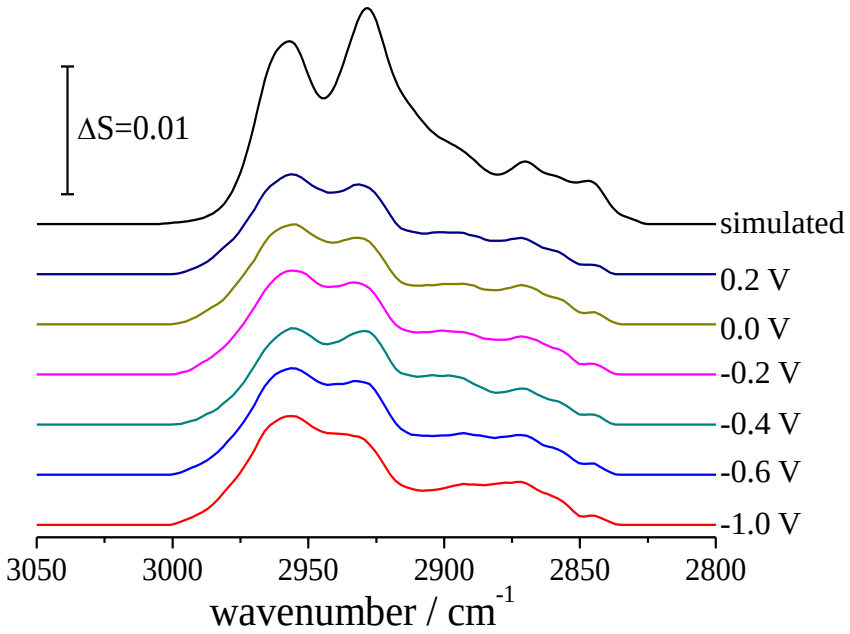


Figure 6. C-H stretching region of the PM-IRRAS spectra of the DPhPC/Alm bilayer floating at the $\beta$-Tg modified gold (111) surface in a 0.1 M NaF/$D_2O$ solution at selected potentials vs. Ag/AgCl. The top line corresponds to the spectrum simulated for a randomly oriented DPhPC/Alm film.

Integrated intensities of the $\nu_s(CH_2)$ and $\nu_{as}(CH_2)$ bands were used to calculate the average orientation of the trans fragments of the diphytanyl chains using procedure described in Ref. [29]. The tilt angles of trans fragments are an approximate measure of the average tilt angle of the acyl chains ($\gamma_{chain}$) and these values have been plotted for the DPhPC and DPhPC/Alm floating bilayers as a function of the electrode potential in Figure 7. In addition, Figure 7 also plots the angle between the direction of the C=O bond and the surface normal ($\theta_{CO}$), which was calculated from the integrated intensity of the C=O stretching band presented in Figure 8. Within experimental error, the angles of $\gamma_{chain}$ and $\theta_{CO}$ are potential independent demonstrating that the orientation of the DPhPC molecules does not change even upon desorption (detachment) of the bilayer from the gold surface and indicating that the bilayers are quite robust. This behavior is typical for a floating bilayer as explained by Matyszewska et al.[32] In a sBLM, the polar head groups reside in the plane of the metal in the attached (adsorbed) state. If the cross sectional area of the polar head group is larger than the cross sectional area of the chains, the chains tilt to ensure efficient packing. At negative potentials, the bilayer is detached and is floating on a cushion of electrolyte. Upon desorption, the head groups can reorganize and pack in a zigzag configuration. The tighter packing of the zigzag configuration induces a reorientation of the lipid tails causing a significant change in the average tilt angle as a function of applied potential. In contrast, the floating bilayer membrane is separated from the metal by a cushion of water molecules in whole range of potentials. There is no significant change in the orientation of the polar head groups of the phospholipids. Consequently, the tilt angle of the lipid tails in the attached and detached states of the bilayer remains unchanged. This is supported by the independence of the tilt angle with potential shown in Figure 7 and indicates that the spacer region of the fBLM must also contain water molecules.

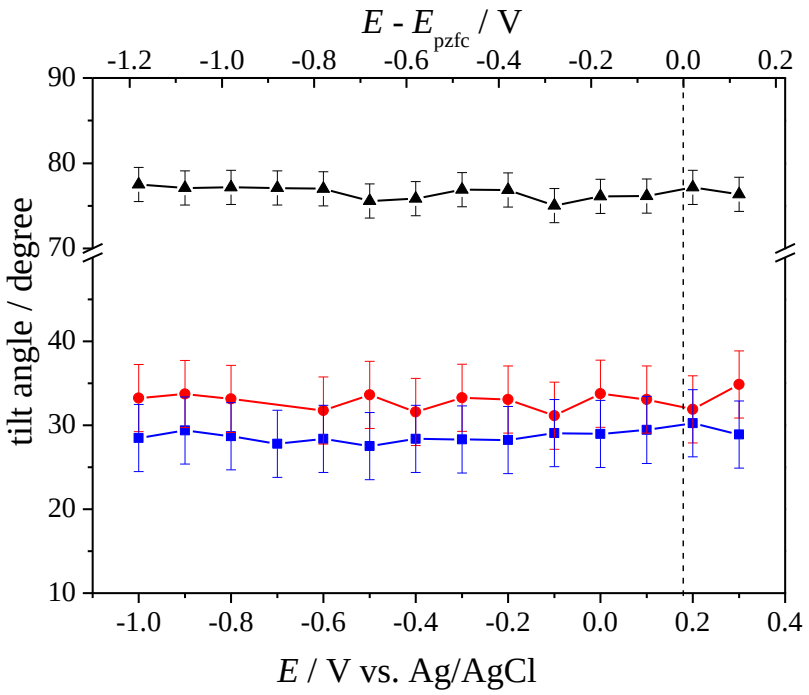


Figure 7. Tilt angles of the DPhPC acyl chains in the pure DPhPC floating bilayer (blue) and the tilt angles of the acyl chains (red circles) and C=O bond (black triangles) of the DPhPC molecules in the DPhPC/Alm floating bilayer as a function of the potential.

The $\gamma_{chain}$ values of the DPhPC/Alm floating bilayer are around 30°, which is close to the values previously reported for the supported bilayer[29] and the angles of $\theta_{CO}$ are close to ~75°. The C=O bond is nearly perpendicular to the fully stretched all-trans acyl chains, therefore, the values of $\gamma_{chain}$ and $\theta_{CO}$ are in good agreement with the structure of the DPhPC molecule. Figure 7 shows that $\gamma_{chain}$ of the DPhPC floating bilayer is slightly larger in the presence of alamethicin. The length of the alamethicin molecule is shorter than the thickness of the hydrophobic region of the DPhPC bilayer.[6, 48] To ensure good hydrophobic matching, insertion of alamethicin leads to a thinning in the DPhPC bilayer,[49] which explains the slight increase in $\gamma_{chain}$ observed in the DPhPC/Alm bilayer. In the surface state, the hydrophobic fragment of alamethicin molecules is imbedded into the hydrophobic core of the membrane and the hydrophilic fragment is oriented towards the solution. Therefore, the imbedded fragment of the peptide would impart a small compressive force onto the hydrophobic

core, which explains the small increase in the tilt angle of the acyl chains ($\gamma_{chain}$) observed at more positive potentials.[49]

### 3.2.2 Amide I region

Figure 8 (A) shows the PM-IRRAS spectra collected for the DPhPC/Alm floating bilayer on the $\beta$-Tg modified gold (111) surface in the 1600 to 1800 $cm^{-1}$ region, which corresponds to the amide I vibration of alamethicin[50] and carbonyl stretching of DPhPC. The intensity of the amide I band increases as the potential is scanned in the negative direction from 0.4 V and reaches a maximum value at -0.5 V vs. Ag/AgCl. At potentials more negative than -0.5 V vs. Ag/AgCl, the intensity begins to decrease and returns to the original value at -1.1 V vs. Ag/AgCl. To assist with the deconvoultion of the broad amide I band, the Fourier self-deconvolution (FSD) and Second Derivative (CD) of the PM-IRRAS spectrum were calculated and plotted in Figure S4 of the Supporting Information. Figure 8 (B) shows the resulting deconvolution of the alamethicin amide I region, which consists of five distinct spectral bands. According to literature, the two strong bands located at 1633 and 1656 $cm^{-1}$ are assigned to the $3_{10}$-helix and $\alpha$-helix, respectively.[29] The band at 1620 $cm^{-1}$ is related to the $\beta$-sheet structure and the two remaining bands positioned at 1646 and 1673 $cm^{-1}$ are associated with the $\beta$-turn structures.[19, 29, 50, 51, 52] The $\beta$-turn structure in alamethicin is a type III $\beta$-turn, which arises from a single turn of the $3_{10}$-helix.[51] The three $\beta$-secondary structure bands are weak, which is consistent with the XRD results showing that the secondary structure of alamethicin is predominantly helical in nature.[6]

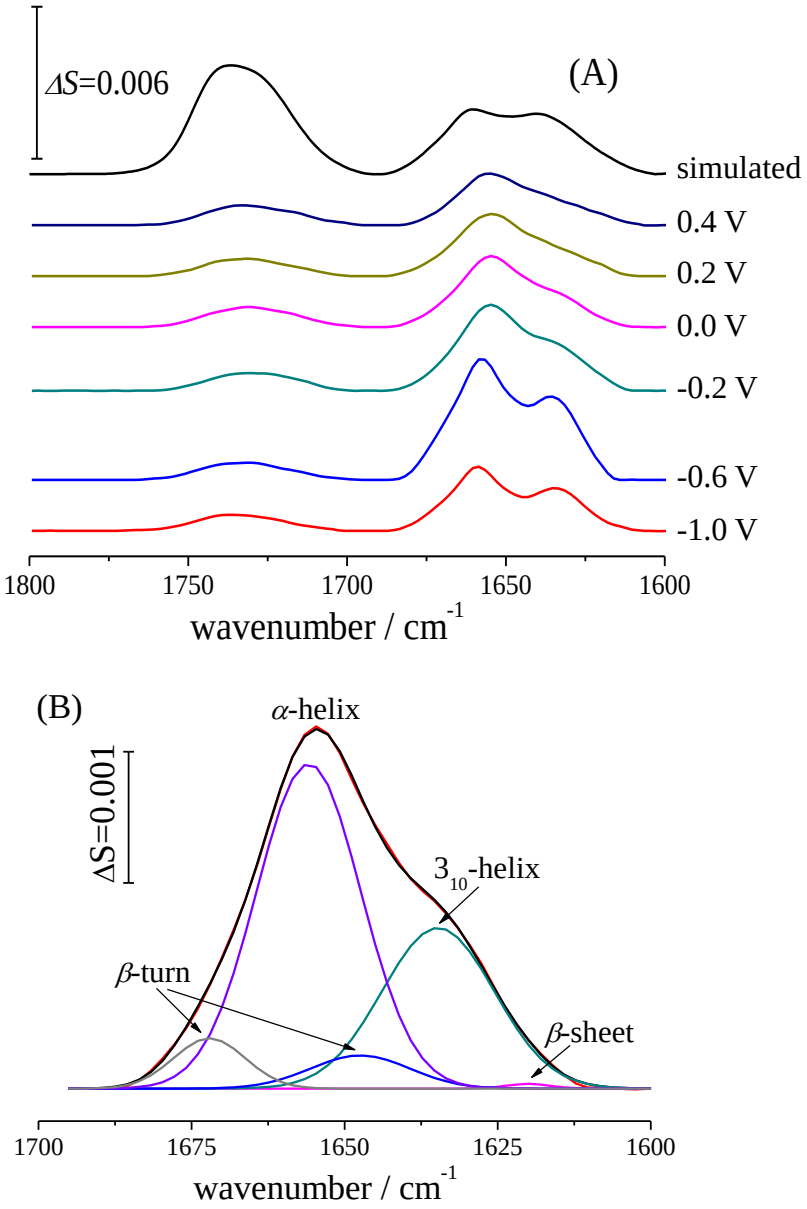


Figure 8. (A) Amide I region of the PM-IRRAS spectra collected for the DPhPC/Alm floating bilayer at the $\beta$-Tg modified gold (111) surface in a 0.1 M NaF/$D_2O$ electrolyte at selected potentials vs. Ag/AgCl. The top curve represents the spectrum that is simulated for a randomly oriented DPhPC/Alm bilayer. (B) Deconvolution of the amide I band of the PM-IRRAS spectrum of the DPhPC/Alm bilayer at $E$ = 0.0 V vs. Ag/AgCl.

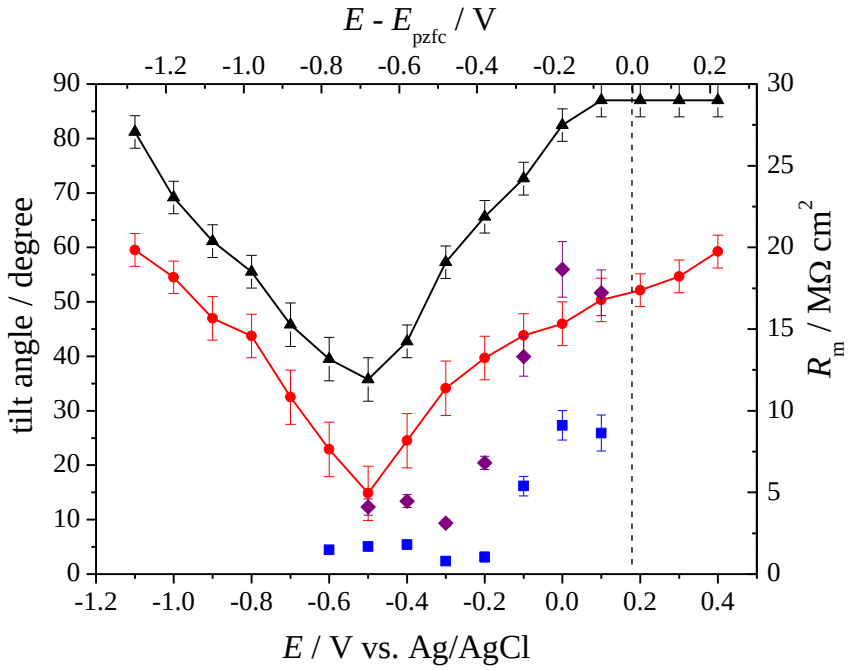


Figure 9. Tilt angle (left axis) of the $3_{10}$-helix (black triangles) and $\alpha$-helix (red circles) of alamethicin in the DPhPC/Alm floating bilayer and the variation in membrane resistance, $R_m$, (right axis) of the pure DPhPC (purple diamonds) and DPhPC/Alm (blue squares) floating bilayers as a function the potential.

The average tilt angles of the $3_{10}$-helix $\gamma(3_{10}\text{-helix})$ and $\alpha$-helix $\gamma(\alpha\text{-helix})$ of alamethicin with respect to the surface normal can be determined from the intensity of the corresponding sub-bands of the amide I band.[29] Figure 9 displays the variation of $\gamma(3_{10}\text{-helix})$ and $\gamma(\alpha\text{-helix})$ as a function both the electrode potential (bottom horizontal axis) and $E\text{-}E_{pzfc}$ (top horizontal axis), which is a measure of the transmembrane potential. The data suggests that the $\gamma(3_{10}\text{-helix})$ and $\gamma(\alpha\text{-helix})$ are strongly potential dependent. For the positive transmembrane potential region ($E\text{-}E_{pzfc} > -0.1$ V), the tilt angle of the $3_{10}$-helix was around $87 \pm 3^o$ and the tilt angle of the $\alpha$-helix was between $50^o$ and $60^o$. These values demonstrate that the alamethicin molecules adopt a weakly inserted orientation or surface state. At transmembrane potentials ($E\text{-}E_{pzfc}$) < -0.2 V, the values of $\gamma(3_{10}\text{-helix})$ and $\gamma(\alpha\text{-helix})$ rapidly decreased as the potential becomes more negative and attained minimum values of $36 \pm 4^o$ and $15 \pm 5^o$ for the $\gamma(3_{10}\text{-helix})$ and $\gamma(\alpha\text{-helix})$, respectively, at a

transmembrane potential of -0.7 V. The low values of $\gamma(3_{10}\text{-helix})$ and $\gamma(\alpha\text{-helix})$ indicate that the alamethicin peptides are inserted into the DPhPC bilayer. The lowering of membrane resistivity, observed in Figure 5 (A), indicates that alamethicin formed ion conduction channels in the inserted peptide state. Direct images of alamethicin ion channels in a floating bilayer were previously observed by Abbasi et al.[24] The tilt angles of alamethicin in the inserted state measured by the PM-IRRAS technique are in good agreement with previously reported values for alamethicin ion channels in the fluid phase of lipid bilayers measured by CD,[53] EPR,[54] NMR,[18] and SEIRAS.[25]

At $(E\text{-}E_{pzfc}) < -0.8$ V, electro-dewetting of the bilayer takes place. The bilayer is progressively lifted from the gold surface[29] and at very negative potentials, the bilayer is floating on a thick cushion of the electrolyte.[43, 44] The $\gamma(3_{10}\text{-helix})$ and $\gamma(\alpha\text{-helix})$ angles increased at these negative potentials. At the transmembrane potential of -1.3 V, the tilt angles of the $3_{10}$-helix and $\alpha$-helix increase to $81^{o} \pm 3^{o}$ and $60^{o} \pm 4^{o}$, respectively, illustrating that alamethicin adopts a surface state when the bilayer is detached from the gold surface. When the bilayer is lifted from the gold surface, the electrolyte penetrates the space between the membrane and the metal surface. As a result, the potential drop occurs between the metal and electrolyte in this spacer region, which consequently leads to a progressive loss in the transmembrane potential. Figure 9 shows that the alamethicin molecules assume a surface state in response to the loss in transmembrane potential. These results demonstrate that the insertion of alamethicin molecules into the membrane is driven by the potential drop across the membrane. The difference between the average angles difference of the $3_{10}$-helix and $\alpha$-helix amounts to $23 \pm 5^{o}$ in the entire range of measured potentials. This value is in good agreement with the literature values, which range from 15 to $25^{o}$ for the helix bend angle caused by the 14-proline residue.[6, 55] This agreement illustrates that the orientation of alamethicin determined by the PM-IRRAS technique are free from major systematic errors.

The open and close states of alamethicin channels are expected to be reversible with respect to the transmembrane potential change.[7] To test the reversibility of the

fBLM, the PM-IRRAS spectra of the DPhPC/Alm floating bilayer were recorded by changing the electrode potential from 0.4 V to -0.6 V vs. Ag/AgCl, and then reversing the potential from -0.6 V to 0.2 V vs. Ag/AgCl. The IR spectra of the amide I region are shown in Figure 10 (A). The spectra demonstrate that the intensity of the amide I band decreases when potential is moved in negative direction and increases when the direction of the potential change is reversed. Figure 10 (B) plots the $\gamma(3_{10}$-helix) and $\gamma(\alpha$-helix) as a function of the applied electrode potential. The angles of $\gamma(3_{10}$-helix) and $\gamma(\alpha$-helix) are decreased when the electrode potential is moved in negative direction. After reaching the negative potential limit at -0.6 V vs. Ag/AgCl, the tilt angles begin to increase during the reverse potential scan and reestablish their original tilt angle values at 0.2 V vs. Ag/AgCl. These findings show that alamethicin inserts into the floating bilayer to form ion channels when the transmembrane potential becomes negative and returns to the surface state when the potential moves back to positive values. The minimum values of $\gamma(3_{10}$-helix) and $\gamma(\alpha$-helix) are reached at the potential of -0.5 V vs. Ag/AgCl (-0.68 V vs. $E$-$E_{pzfc}$). The findings of this experiment proves that the potential controlled insertion of alamethicin is reversible and demonstrates that the peptide prefers the surface in the absence of a sufficiently strong electric field where the hydrophilic fragment interacts with water and the hydrophobic portion interacts with the membrane.[16, 56, 57]

The pores formed by membrane active peptides may adopt either toroidal[58] or barrel-stave[59] structures. In the toroidal model, the head groups of the lipid molecules tilt towards the central hole, so that the pore walls used to establish the water core are lined with the inserted peptides and lipid head groups. Therefore, toroidal pore models would cause a significant change in the orientation of the lipid molecules. In the barrel-stave model, transmembrane pores are created by the aggregation of the peptide with the hydrophobic subunits aligned towards the lipid core and hydrophilic segments directed towards the water core. As a result, barrel-stave pores are formed without significant reorientation of the lipid molecules. The PM-IRRAS results show that when the alamethicin peptides transition from the surface to inserted into the membrane at negative potentials, the average tilt of the acyl lipid chains and the

direction of the C=O transition dipole of DPhPC remain unchanged. This evidence suggests that alamethicin forms barrel-stave type pores in the DPhPC floating bilayer.[8, 9]

Figure 11 compares the tilt angles of the alamethicin $\alpha$-helix and membrane resistance for the floating bilayer from this work with the values of the solid supported bilayer reported in a recent study.[29] Surprisingly, the agreement between the data from the floating and supported bilayers is very close. This agreement implies that the alamethicin peptides in the DPhPC/Alm supported bilayer are not denatured when the bilayer is in direct contact with the gold surface. This behavior is in contrast to the properties of gramicidin A where the $\beta$-helix is stressed in sBLM[60] and stress is released in the fBLM.[61] The similar properties of alamethicin in the two bilayers are characteristic for this peptide and should not be interpreted as insufficient amount of water in the spacer region or a reduction in the membrane mobility.

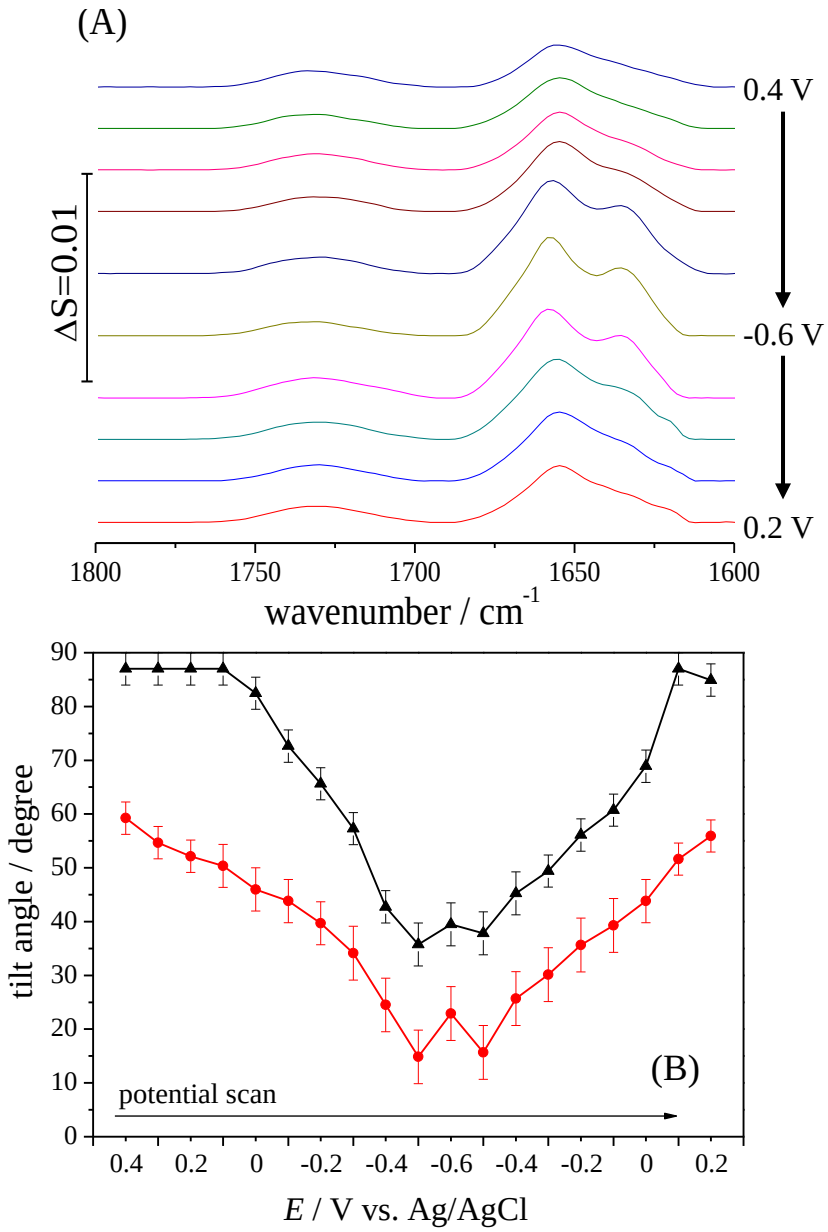


Figure 10. (A) PM-IRRAS spectra for the amide I stretching region of the DPhPC/Alm floating bilayer on the $\beta$-Tg modified gold (111) surface by scanning the potential in the negative direction from an initial potential of 0.4 V (top spectrum) to -0.6 V vs. Ag/AgCl and then positively from -0.6 to 0.2 V vs. Ag/AgCl. (B) Tilt angles of the $3_{10}$-helix (black triangles) and $\alpha$-helix (red circles) of alamethicin as the potential is scanned in the negative potential from 0.4 to -0.6 V vs. Ag/AgCl and then reversing the potential and scanning the voltage in the positive direction from -0.6 to 0.2 V vs. Ag/AgCl (left to right on x-axis).

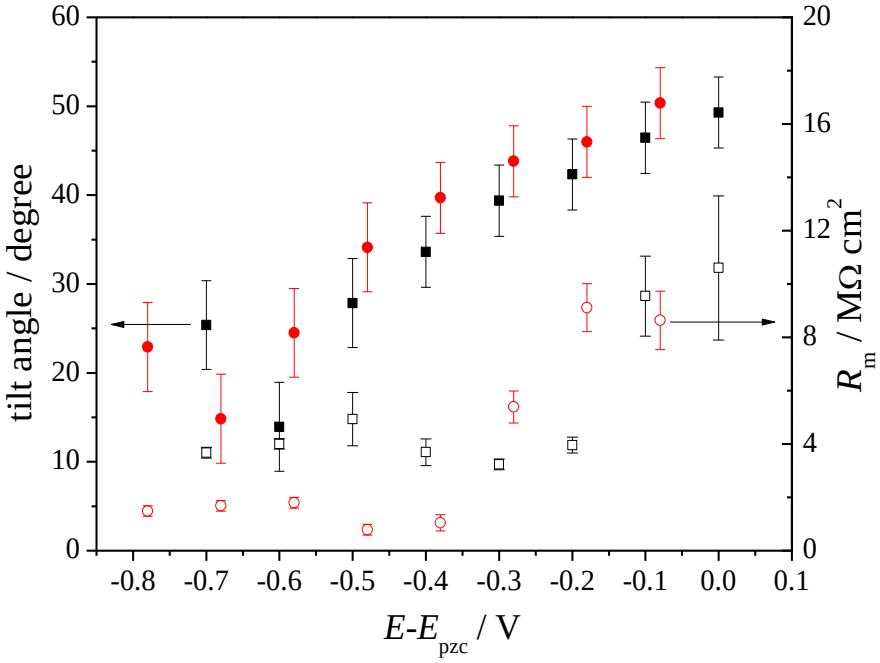


Figure 11. Tilt angles of the $\alpha$-helix (filled symbols, left y-axis) and membrane resistance (empty symbols, right y-axis) of the DPhPC/Alm fBLM (red circles) and DPhPC/Alm sBLM (black rectangles) as a function of the transmembrane potential.

The electrochemical and PM-IRRAS results clearly illustrate that the insertion of alamethicin into the two bilayers is driven by the negative electric field across the bilayer. In previous paper devoted to DPhPC sBLMs,[29] we applied the model proposed by Guidelli and Becucci[16] to interpret our results. This model assumes that the insertion is driven by the field-dipole interactions followed by the aggregation of alamethicin to form an ion conducting pore. However, the potential dependent insertion of alamethicin into the sBLM and fBLM is contradictory to a recent study of alamethicin in a tethered bilayer (tBLM).[30] In contrast to behavior of alamethicin in the sBLM[29] and in mercury supported model membranes,[62] the orientation of the inserted alamethicin peptides in the tBLM was potential independent, which is a puzzling result. To understand the difference in the barrier properties of these model membranes in the absence of the alamethicin, the EIS phase angles of the fBLM, sBLM and tBLM are plotted in Figure 12.

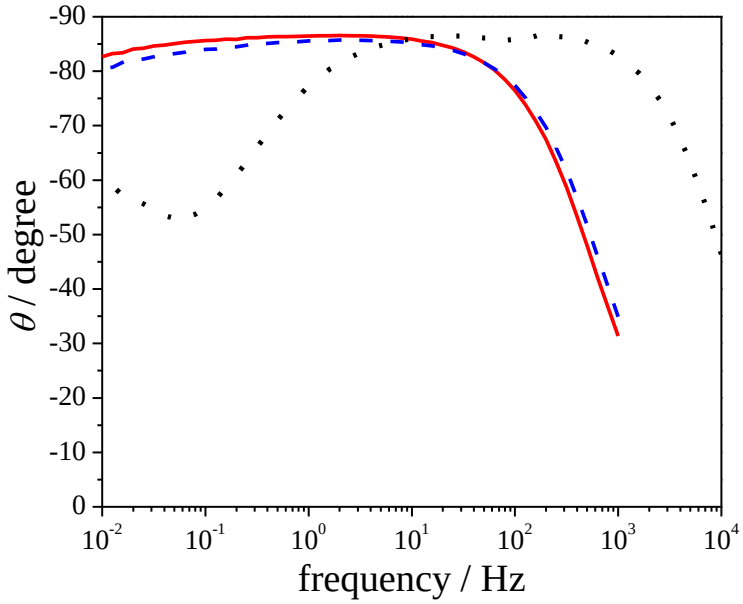


Figure 12. Phase angle plots of the DPhPC fBLM at 0.1 V vs. Ag/AgCl (red solid), DPhPC sBLM at 0.1 V vs. Ag/AgCl (blue dashed) and DPhPC/DPTL tBLM at 0.2 V vs. Ag/AgCl (black dotted).

The shapes of the phase angle curves for the sBLM and fBLM are quite similar. However, they are both drastically different than the tBLM model membrane, which displays a minimum at low frequencies. Valincius et al.[41,42] have demonstrated that the appearance of a minimum is due to the presence of defects in the bilayer and the frequency position is correlated to the defect density. The sBLM and fBLM display only small decrease in the phase angle at low frequencies, while the tBLM decreases from 85° to 55° at ~0.05 Hz. This behavior indicates that the tBLM has a significantly higher density of defects than the fBLM and sBLM. The corresponding $R_m$ values amount to 10.6 ± 2.7 MΩ cm$^2$ for sBLM, 8.6 ± 1.1 MΩ cm$^2$ for fBLM and 0.66 ± 0.08 MΩ cm$^2$ for tBLM. The membrane resistivity is an order of magnitude lower for tBLM than for of sBLM or fBLM. Additionally, the phase angles for tBLM are much higher than the sBLM and fBLM at high frequencies. This is a manifestation of a much lower capacitance of the tBLM membrane.[30] These data sets demonstrate that insertion of alamethicin into the membrane depends strongly on the presence of defects in the bilayer. Membranes with a high defect density allow the peptides penetrate easily into the bilayer resulting in a weak voltage dependency. The lack of

dependence on the electrode potential may be a result of either low mobility of peptide molecules in the tethered bilayer or to a high density of defects. The latter allows a large number of ions to penetrate the bilayer and enter the spacer region between the membrane and metal surface, which results in a loss of the transmembrane potential. The present studies show that defect density is low for sBLM and fBLM. However, positive correlations between potential controlled changes in the resistance of membranes in the absence and presence of alamethicin, shown in Figure 5, indicate that the peptide insertion is assisted by electroporation of the bilayer, which occurs at negative potentials. The role of defects in assisting incorporation of amphiphilic peptides into phospholipid bilayers was recently described by Murayama et al.[63] This conclusion is also consistent with the work by Cranfield et al.,[64] who demonstrated that pulses of negative transmembrane potential with absolute amplitude higher than 0.15 V caused electroporation of a tethered bilayer and assisted incorporation of an amphiphilic peptide into the bilayer. The present studies provided important information about the impact of electroporation on incorporation of peptides into metal supported and floating bilayers. They demonstrate that electroporation or defect-assisted peptide incorporation into biomimetic membranes is a general phenomenon.

## Conclusion

Electrochemical methods and PM-IRRAS technique were employed to study the ion channel properties of alamethicin incorporated in the DPhPC floating bilayer at the $\beta$-Tg modified gold (111) surface. The results illustrate that the alamethicin forms ion channels at transmembrane potentials more negative than -0.15 V. At more positive transmembrane potentials, alamethicin molecules reside on the bilayer surface (surface state). The present data confirms that the insertion of alamethicin into a model membrane is voltage driven. However, these studies also indicate that peptide insertion is assisted by electroporation of the bilayer at negative potentials. This work illustrates the significance of defects on the permeabilization of biomimetic

membranes by antimicrobial peptides.

## Acknowledgements

This work was supported by a grant from Natural Sciences and Engineering Research Council of Canada (NSERC) (RG-03958).

## Supporting Information

The immersion current transients; EIS data of the DPhPC floating bilayer at different potentials; the models chosen to fit the EIS data of the DPhPC floating bilayer; FSD and SD results of the PM-IRRAS spectrum; numerical values of the elements in the equivalent circuit of DPhPC/Alm bilayers and DPhPC bilayers

## References:

1. Brogden, K. A. Antimicrobial peptides: pore formers or metabolic inhibitors in bacteria? *Nat. Rev. Microbiol.* **2005,** *3* (3), 238.

2. Reddy, K.; Yedery, R.; Aranha, C. Antimicrobial peptides: premises and promises. *Int J Antimicrob Agents* **2004,** *24* (6), 536-547.

3. Zasloff, M. Antimicrobial peptides of multicellular organisms. *Nature* **2002,** *415* (6870), 389-395.

4. Meyer, C. E.; Reusser, F. A polypeptide antibacterial agent isolated fromTrichoderma viride. *Experientia* **1967,** *23* (2), 85-86.

5. Sakmann, B.; Boheim, G. Alamethicin-induced single channel conductance fluctuations in biological membranes. *Nature* **1979,** *282* (5736), 336-339.

6. Fox Jr, R. O.; Richards, F. M. A voltage-gated ion channel model inferred from the crystal structure of alamethicin at 1.5-Å resolution. *Nature* **1982,** *300* (5890), 325.

7. Woolley, G. A.; Wallace, B. Model ion channels: gramicidin and alamethicin. *J. Membr. Biol.* **1992,** *129* (2), 109-136.

8. He, K.; Ludtke, S. J.; Worcester, D. L.; Huang, H. W. Neutron scattering in the plane of membranes: Structure of alamethicin pores. *Biophys. J.* **1996,** *70* (6), 2659-2666.

9. Chen, F. Y.; Lee, M. T.; Huang, H. W. Sigmoidal concentration dependence of antimicrobial peptide activities: A case study on alamethicin. *Biophys. J.* **2002,** *82* (2), 908-914.

10. Huang, H. W. Molecular mechanism of antimicrobial peptides: The origin of cooperativity. *Biochim. Biophys. Acta* **2006,** *1758* (9), 1292-1302.

11. Pan, J.; Tristram-Nagle, S.; Nagle, J. F. Alamethicin aggregation in lipid membranes. *J. Membr. Biol.* **2009,** *231* (1), 11.

12. Salditt, T.; Li, C.; Spaar, A. Structure of antimicrobial peptides and lipid membranes probed

by interface-sensitive X-ray scattering. *Biochim. Biophys. Acta* **2006,** *1758* (9), 1483-1498.

13. Constantin, D.; Brotons, G.; Jarre, A.; Li, C.; Salditt, T. Interaction of alamethicin pores in DMPC bilayers. *Biophys. J.* **2007,** *92* (11), 3978-3987.

14. Li, C.; Salditt, T. Structure of magainin and alamethicin in model membranes studied by X-ray reflectivity. *Biophys. J.* **2006,** *91* (9), 3285-3300.

15. Becucci, L.; Guidelli, R.; Peggion, C.; Toniolo, C.; Moncelli, M. R. Incorporation of channel-forming peptides in a Hg-supported lipid bilayer. *J. Electroanal. Chem.* **2005,** *576* (1), 121-128.

16. Guidelli, R.; Becucci, L. Mechanism of voltage-gated channel formation in lipid membranes. *Biochim. Biophys. Acta* **2016,** *1858* (4), 748-755.

17. Marsh, D. Orientation and Peptide-Lipid Interactions of Alamethicin Incorporated in Phospholipid Membranes: Polarized Infrared and Spin-Label EPR Spectroscopy. *Biochemistry* **2009,** *48* (4), 729-737.

18. Bak, M.; Bywater, R. P.; Hohwy, M.; Thomsen, J. K.; Adelhorst, K.; Jakobsen, H. J.; Sorensen, O. W.; Nielsen, N. C. Conformation of alamethicin in oriented phospholipid bilayers determined by N-15 solid-state nuclear magnetic resonance. *Biophys. J.* **2001,** *81* (3), 1684-1698.

19. Ye, S.; Nguyen, K. T.; Chen, Z. Interactions of alamethicin with model cell membranes investigated using sum frequency generation vibrational spectroscopy in real time in situ. *J. Phys. Chem. B* **2010,** *114* (9), 3334-3340.

20. Ye, S.; Li, H.; Wei, F.; Jasensky, J.; Boughton, A. P.; Yang, P.; Chen, Z. Observing a model ion channel gating action in model cell membranes in real time in situ: membrane potential change induced alamethicin orientation change. *J. Am. Chem. Soc.* **2012,** *134* (14), 6237-6243.

21. Yang, P.; Wu, F.-G.; Chen, Z. Lipid fluid-gel phase transition induced alamethicin orientational change probed by sum frequency generation vibrational spectroscopy. *J. Phys. Chem. C* **2013,** *117* (33), 17039-17049.

22. Yang, P.; Wu, F.-G.; Chen, Z. Dependence of alamethicin membrane orientation on the solution concentration. *J. Phys. Chem. C* **2013,** *117* (7), 3358-3365.

23. Pieta, P.; Mirza, J.; Lipkowski, J. Direct visualization of the alamethicin pore formed in a planar phospholipid matrix. *Proc. Nat.l Acad. Sci. USA* **2012,** *109* (52), 21223-21227.

24. Abbasi, F.; Leitch, J. J.; Su, Z.; Szymanski, G.; Lipkowski, J. Direct visualization of alamethicin ion pores formed in a floating phospholipid membrane supported on a gold electrode surface. *Electrochimica Acta* **2018,** *267*, 195-205.

25. Forbrig, E.; Staffa, J. K.; Salewski, J.; Mroginski, M. A.; Hildebrandt, P.; Kozuch, J. Monitoring the orientational changes of alamethicin incorporating into bilayer lipid membranes. *Langmuir* **2018,** *34*, 2373-2385.

26. Jiang, X.; Zaitseva, E.; Schmidt, M.; Siebert, F.; Engelhard, M.; Schlesinger, R.; Ataka, K.; Vogel, R.; Heberle, J. Resolving voltage-dependent structural changes of a membrane photoreceptor by surface-enhanced IR difference spectroscopy. *Proc. Nat.l Acad. Sci. USA* **2008,** *105* (34), 12113-12117.

27. Lipkowski, J. Building biomimetic membrane at a gold electrode surface. *Phys. Chem. Chem. Phys.* **2010,** *12* (42), 13874-13887.

28. Kycia, A. H.; Su, Z.; Brosseau, C. L.; Lipkowski, J. In Situ PM–IRRAS Studies of Biomimetic Membranes Supported at Gold Electrode Surfaces. In *Vibrational Spectroscopy at Electrified Interfaces*, Wieckowski, A.; Korzeniewski, C.; Braunschweig, B., Eds.; Wiley-VCH:

Weinheim, 2013, pp 345-417.

29. Su, Z.; Shodiev, M.; Leitch, J. J.; Abbasi, F.; Lipkowski, J. In situ electrochemical and PM-IRRAS studies of ion channels formation by alamethicin in model phospholipid bilayers. *J. Electroanal. Chem.* **2017**, DOI: 10.1016/j.jelechem.2017.10.042.

30. Su, Z.; Leitch, J. J.; Abbasi, F.; Faragher, R. J.; Schwan, A. L.; Lipkowski, J. EIS and PM-IRRAS studies of alamethicin ion channels in a tethered lipid bilayer. *J. Electroanal. Chem.* **2018,** *812*, 213-220.

31. Kycia, A. H.; Wang, J.; Merrill, A. R.; Lipkowski, J. Atomic force microscopy studies of a floating-bilayer lipid membrane on a Au (111) surface modified with a hydrophilic monolayer. *Langmuir* **2011,** *27* (17), 10867-10877.

32. Matyszewska, D.; Bilewicz, R.; Su, Z.; Abbasi, F.; Leitch, J. J.; Lipkowski, J. PM-IRRAS studies of DMPC bilayers supported on Au (111) electrodes modified with hydrophilic monolayers of thioglucose. *Langmuir* **2016,** *32* (7), 1791-1798.

33. Richer, J.; Lipkowski, J. Measurement of physical adsorption of neutral organic species at solid electrodes. *J. Electrochem. Soc.* **1986,** *133* (1), 121-128.

34. Hamm, U.; Kramer, D.; Zhai, R.; Kolb, D. The pzc of Au (111) and Pt (111) in a perchloric acid solution: an ex situ approach to the immersion technique. *J. Electroanal. Chem.* **1996,** *414* (1), 85-89.

35. Su, Z.; Leitch, J.; Lipkowski, J. Measurements of the potentials of zero free charge and zero total charge for 1-thio-±bβ-D-glucose and DPTL modified Au (111) surface in different electrolyte solutions. *Z. Phys. Chem.* **2012,** *226* (9-10), 995-1009.

36. Zamlynny, V. Electrochemical and spectroscopy studies of pyridine surfactants at the gold-electrolyte interface. PhD thesis, University of Guelph, Canada, 2002.

37. Zawisza, I.; Bin, X.; Lipkowski, J. Potential-driven structural changes in Langmuir-Blodgett DMPC bilayers determined by in situ spectroelectrochemical PM IRRAS. *Langmuir* **2007,** *23* (9), 5180-5194.

38. Valincius, G.; McGillivray, D. J.; Febo-Ayala, W.; Vanderah, D. J.; Kasianowicz, J. J.; Lösche, M. Enzyme activity to augment the characterization of tethered bilayer membranes. *J. Phys. Chem. B* **2006,** *110* (21), 10213-10216.

39. McGillivray, D. J.; Valincius, G.; Vanderah, D. J.; Febo-Ayala, W.; Woodward, J. T.; Heinrich, F.; Kasianowicz, J. J.; Löscheb, M. Molecular-scale structural and functional characterization of sparsely tethered bilayer lipid membranes. *Biointerphases* **2007,** *2* (1), 21-33.

40. McGillivray, D. J.; Valincius, G.; Heinrich, F.; Robertson, J. W.; Vanderah, D. J.; Febo-Ayala, W.; Ignatjev, I.; Lösche, M.; Kasianowicz, J. J. Structure of functional Staphylococcus aureus α-hemolysin channels in tethered bilayer lipid membranes. *Biophys. J.* **2009,** *96* (4), 1547-1553.

41. Valincius, G.; Meškauskas, T.; Ivanauskas, F. Electrochemical impedance spectroscopy of tethered bilayer membranes. *Langmuir* **2012,** *28* (1), 977-990.

42. Valincius, G.; Mickevicius, M. Tethered phospholipid bilayer membranes: an interpretation of the electrochemical impedance response. In *Advances in Planar Lipid Bilayers and Liposomes*; Elsevier, 2015; Vol. 21, pp 27-61.

43. Burgess, I.; Li, M.; Horswell, S.; Szymanski, G.; Lipkowski, J.; Majewski, J.; Satija, S. Electric field-driven transformations of a supported model biological membrane—an electrochemical and neutron reflectivity study. *Biophys. J.* **2004,** *86* (3), 1763-1776.

44. Uchida, T.; Osawa, M.; Lipkowski, J. SEIRAS studies of water structure at the gold

electrode surface in the presence of supported lipid bilayer. *J. Electroanal. Chem.* **2014,** *716*, 112-119.

45. Leitch, J.; Kunze, J.; Goddard, J. D.; Schwan, A. L.; Faragher, R. J.; Naumann, R.; Knoll, W.; Dutcher, J. R.; Lipkowski, J. In situ PM-IRRAS studies of an archaea analogue thiolipid assembled on a au(111) electrode surface. *Langmuir* **2009,** *25* (17), 10354-10363.

46. Casal, H. L.; Mantsch, H. H. Polymorphic phase behavior of phospholipid membranes studied by infrared spectroscopy. *Biochim. Biophys. Acta* **1984,** *779* (4), 381-401.

47. Lindsey, H.; Petersen, N. O.; Chan, S. I. Physicochemical characterization of 1,2-diphytanoyl-sn-glycero-3-phosphocholine in model membrane systems. *Biochim. Biophys. Acta* **1979,** *555* (1), 147-167.

48. Nagle, J. F.; Tristram-Nagle, S. Structure of lipid bilayers. *Biochim. Biophys. Acta* **2000,** *1469* (3), 159-195.

49. He, K.; Ludtke, S. J.; Heller, W. T.; Huang, H. W. Mechanism of alamethicin insertion into lipid bilayers. *Biophys. J.* **1996,** *71* (5), 2669-2679.

50. Haris, P. I.; Chapman, D. Fourier transform infrared spectra of the polypeptide alamethicin and a possible structural similarity with bacteriorhodopsin. *Biochim. Biophys. Acta* **1988,** *943* (2), 375-380.

51. Kennedy, D.; Crisma, M.; Toniolo, C.; Chapman, D. Studies of peptides forming 310-and. alpha.-helixes and. beta.-bend ribbon structures in organic solution and in model biomembranes by Fourier transform infrared spectroscopy. *Biochemistry* **1991,** *30* (26), 6541-6548.

52. Haris, P. I.; Molle, G.; Duclohier, H. Conformational changes in alamethicin associated with substitution of its α-methylalanines with leucines: A FTIR spectroscopic analysis and correlation with channel kinetics. *Biophys. J.* **2004,** *86* (1), 248-253.

53. Vogel, H. Comparison of the Conformation and Orientation of Alamethicin and Melittin in Lipid Membranes. *Biochemistry* **1987,** *26* (14), 4562-4572.

54. Marsh, D.; Jost, M.; Peggion, C.; Toniolo, C. TOAC spin labels in the backbone of alamethicin: EPR studies in lipid membranes. *Biophys J* **2007,** *92* (2), 473-481.

55. Nagao, T.; Mishima, D.; Javkhlantugs, N.; Wang, J.; Ishioka, D.; Yokota, K.; Norisada, K.; Kawamura, I.; Ueda, K.; Naito, A. Structure and orientation of antibiotic peptide alamethicin in phospholipid bilayers as revealed by chemical shift oscillation analysis of solid state nuclear magnetic resonance and molecular dynamics simulation. *Biochim. Biophys. Acta* **2015,** *1848* (11), 2789-2798.

56. Eisenberg, M.; Hall, J. E.; Mead, C. The nature of the voltage-dependent conductance induced by alamethicin in black lipid membranes. *J. Membr. Biol.* **1973,** *14* (1), 143-176.

57. Vodyanoy, I.; Hall, J.; Balasubramanian, T. Alamethicin-induced current-voltage curve asymmetry in lipid bilayers. *Biophys. J.* **1983,** *42* (1), 71-82.

58. Matsuzaki, K.; Murase, O.; Fujii, N.; Miyajima, K. An antimicrobial peptide, magainin 2, induced rapid flip-flop of phospholipids coupled with pore formation and peptide translocation. *Biochemistry* **1996,** *35* (35), 11361-11368.

59. Yang, L.; Harroun, T. A.; Weiss, T. M.; Ding, L.; Huang, H. W. Barrel-stave model or toroidal model? A case study on melittin pores. *Biophys. J.* **2001,** *81* (3), 1475-1485.

60. Laredo, T.; Dutcher, J. R.; Lipkowski, J. Electric field driven changes of a gramicidin containing lipid bilayer supported on a Au (111) surface. *Langmuir* **2011,** *27* (16), 10072-10087.

61. Goodall, B. L. Surface analytical studies of Gramicidin A in biomimetic model membrane systems. Master thesis, University of Guelph, Canada, 2014.

62. Becucci, L.; Guidelli, R. What ion flow along ion channels can tell us about their functional

activity. *Membranes* **2016,** *6* (4), 53.

63. Murayama, T.; Masuda, T.; Afonin, S.; Kawano, K.; Takatani‐Nakase, T.; Ida, H.; Takahashi, Y.; Fukuma, T.; Ulrich, A. S.; Futaki, S. Loosening of lipid packing promotes oligoarginine entry into cells. *Angew. Chem. Int. Ed.* **2017,** *56* (26), 7644-7647.

64. Cranfield, C. G.; Cornell, B. A.; Grage, S. L.; Duckworth, P.; Carne, S.; Ulrich, A. S.; Martinac, B. Transient potential gradients and impedance measures of tethered bilayer lipid membranes: Pore-forming peptide insertion and the effect of electroporation. *Biophys. J.* **2014,** *106* (1), 182-189.

TOC Table of contents graphics